Available online at www.sciencedirect.com
ScienceDirect
International Journal of Heat and Mass Transfer 50 (2007) 1762–1770
International Journal of HEAT and MASS TRANSFER
www.elsevier.com/locate/ijhmt

Three-dimensional condensation regime diagram for direct contact condensation of steam injected into water

A. Petrovic de With [a,*], R.K. Calay [a], G. de With [b,1]

[a] Fluid Mechanics Research Group, University of Hertfordshire, College Lane, Hatfield AL10 9AB, UK
[b] Lafarge Roofing Technical Centers Ltd., Sussex Manor Business Park, Gatwick Road, Crawley RH10 9NZ, UK

Received 2 June 2006
Available online 22 December 2006

Abstract

Direct contact condensation (DCC) of steam in water occurs in many industrial devices. Crucial to obtain an appropriate design of the device is an accurate understanding and prediction of the condensation regimes. The two-dimensional regime maps presently available are able to predict different condensation regimes for limited flow conditions, but fail to predict regimes accurately if a different injector size is considered. In this paper, a new three-dimensional regime diagram is presented, and validated against experiments. Furthermore, corrections necessary to adopt the regime diagram for steam injection into a water flow are discussed in the paper.

PACS: 47.27.Wg; 64.70.Fx; 68.03.Fg

Keywords: Steam; Direct contact condensation; Regimes; Regime map

1. Introduction

Direct Contact Condensation (DCC) of steam in water occurs when steam is introduced into water. It is a phenomenon of high importance used in devices for nuclear, chemical, and marine industry. However, at present there is still limited knowledge on the subject of DCC. The behaviour of DCC is investigated in various experimental studies [1–7] and while this has resulted in a substantial increase in experimental data, a generic understanding of condensation of steam in water is still very limited [8–11].

When steam is injected into water through an injector, an area of steam occurs behind the exit of the injector. This area is the so-called steam plume and its behaviour is very sensitive to steam and water conditions as well as injector shape and size. For example, at a high steam inflow and minimal water subcooling, the steam will bubble through the water as if it is a non-condensable gas. Alternatively, if the steam inflow is very low the steam plume is reduced to a small film in the vicinity of the injector exit [12]. This complicated behaviour of steam is typical for DCC and makes accurate prediction of the steam plume difficult to achieve. Nevertheless, accurate prediction of the steam plume is essential to allow for realistic prediction of the downstream flow behaviour. The geometrical shape as well as the dynamic flow features seen in the steam plume determine the rate with which condensation into water takes place. It is this rate of condensation that determines the transfer of heat into kinetic energy; hence, the prediction of the downstream flow field and all its relevant flow features rely on an accurate prediction of the steam plume. Furthermore, the steam plume shape and behaviour are crucial in the numerical modelling of the process [13].

The most descriptive information about the steam plume behaviour is found in a regime map. In a regime map the steam plume behaviour is called regime and is

* Corresponding author. Tel.: +44 1707 284124; fax: +44 1707 285086.
E-mail addresses: a.de-with@herts.ac.uk (A. Petrovic de With), r.k.calay@herts.ac.uk (R.K. Calay), govert.de.with@lafarge-roofing.com (G. de With).
[1] Tel.: +44 1293 596309; fax: +44 1293 596427.

0017-9310/$ - see front matter © 2006 Elsevier Ltd. All rights reserved.
doi:10.1016/j.ijheatmasstransfer.2006.10.017

Nomenclature

D	diameter of steam injector	*Subscripts*	
G	normalised steam mass flow rate	s	steam
T	temperature	w	water
ΔT	temperature of water subcooling	0	initial conditions/at the injector

described in terms of its geometric appearance and its dynamic features. Until now researchers used experimental data to construct two-dimensional regime maps. These regime maps show the dependence of regimes based on the water subcooling and the steam mass inflow rate. The water subcooling is the temperature difference between steam and surrounding water, while steam mass inflow rate is a spatially and temporally normalised steam inflow. Regime maps were proposed by Liang and Griffith [3], for steam injected through an injector with a diameter $D = 0.02$ m. Aya and Nariai [14,15] proposed a regime map for steam injected through injectors with diameters in the range of $D = 0.009$ m to $D = 0.038$ m. Furthermore Chan and Lee [2], constructed a map for a steam injector with diameter $D = 0.051$ m. In addition, two other regime maps were presented by Block [12] and Chan and Lee [2]. Block [12] presented a regime map, which was originally taken from Chan and Lee [2], but used a different notation of the regimes. Block based his notation on the pressure variation in the water into which steam was injected. Also the regime map, presented by Youn et al. [5] is based on pressure variation in the water. All presented maps were accurate, but valid only for a limited range of flow conditions. Consequently, the regime maps are not suitable if other flow conditions or other injectors are considered. The regime maps may well indicate similar regimes, nevertheless, the corresponding steam inflow rate and temperature subcooling can differ significantly. The ramifications of this are very significant as a well controlled and accurate prediction of the regime is essential for a range of applications where DCC is the dominant flow feature. For this reason there is a distinct need for more generalised predictions of the condensation regime that is accurate across a wide range of flow conditions and injector sizes. It is the aim of this work to present a regime diagram which has this capability.

In this paper a new Three-Dimensional Condensation Regime diagram (3DCR diagram) is presented. The diagram is constructed using the traditional dependencies of water subcooling and steam mass inflow rate. In addition a third dependency is introduced in the form of an injector diameter to account for the injection device. The new 3DCR diagram was constructed from experimental data available in literature. The experimental data is obtained from a comprehensive set of independent experimental studies that has been published during the last three decades. The paper will discuss in detail construction of the new 3DCR diagram and the used experimental data. Further experimental data from a range of independent published sources is used for validation of the diagram. Modifications in the 3DCR diagram to enhance its functionality and to allow for prediction of condensation of steam in water flow are discussed. Validation of this enhanced functionality is done using detailed experiments of DCC. The experiments are performed in connection with this study and are part of an internationally funded project on ballast water.

2. Regions and regimes of DCC

Independent of the condensation regime the process of condensation always consists of four different regions. The first region consists of pure steam and is called the steam plume. The plumes outer surface is the interface, where DCC starts to take place. Surrounding the interface is a hot water layer, which contains of steam bubbles and is characterised by an increase in water temperature. The hot water layer is surrounded by water into which steam is injected and a two-phase jet is formed in the water behind the steam plume. Specific behaviour and a clear appearance of each region may differ depending on the regime. Nevertheless, each region is present when there is a condensation of steam into water.

Fig. 1 shows a photograph of the direct contact condensation of steam. The photograph is obtained from an experiment that is carried out in connection with the presented study. In the experiment 2652 kg/(m^2 s) of steam was injected through an injector with 2 mm diameter into a water flow with a centerline velocity of 1.9 m/s. The temperature difference between injected steam and water flow was 85 °C. Close to the steam injector exit is clearly seen a white ellipsoidal steam plume. Behind the steam plume, a well developed two phase jet can be observed. Below the photograph a schematic drawing of the four different regions is presented.

2.1. Regions of DCC

The steam plume is the first region in the condensation process and occurs at the steam pipe exit. In most computational models the steam plume is approximated by a pure steam region with temperature and velocity gradients in both downstream and radial directions [1,4]. The shape of the steam plume is predominantly dependent on the inflow conditions. A range of steam plume shapes are observed during experimental observations and include:

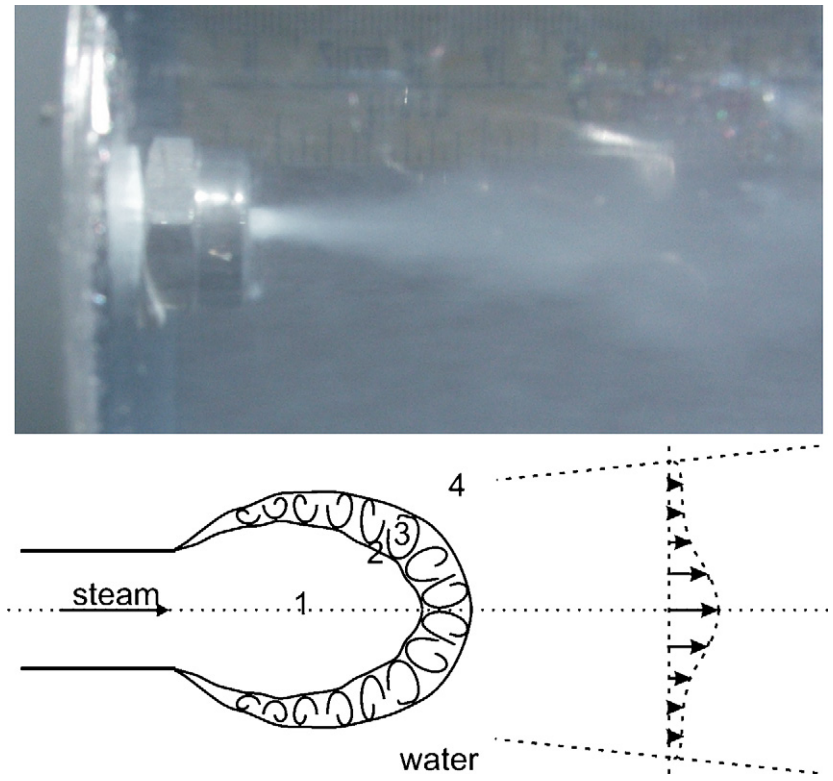

Fig. 1. Photograph of DCC taken during experiments and schematic figure, presenting different regions of DCC of steam injected into water: steam plume (1), interface (2), hot water layer (3) and surrounding water (4). A velocity profile of a developed jet is marked in the surrounding water. Photograph and schematic drawing are not to scale.

hemispherical, conical, ellipsoidal and divergent shape. Alternatively a steam plume in the shape of a bubble can be observed and with very low rates of steam inflow the plume is reduced to a small film covering the injector exit [8,10,16].

The surface of the steam plume or interface, divides the steam from a hot water layer. It is the region where DCC occurs in the form of a convective heat and mass transfer through the interface. The size of the interface is related to the amount of condensed steam. The exact shape and position of the interface are difficult to define. As suggested by Liang and Griffith [3], the exact shape of the interface depends on the interfacial eddies and the local temperature in the hot water layer that surrounds the interface.

The size of the interface depends on the rate of condensation and it also affects this rate. If the interface is small, heat and mass transfer can only take place across a small area and condensation will be comparatively slow. If the steam plume is large, the interface is larger and the condensation will be accelerated. Fast condensation across the interface of a plume increases the instability leading to a collapse of the bubble when the steam supply is insufficient to keep up with the rate of condensation.

The hot water layer or bulk water is a two-phase layer in the vicinity of the interface with a temperature close to saturation. The flow at the interface is mixed with bubbles and there is a large activity of turbulent motion. The turbulence is formed by the momentum subtracted from the condensing steam and has a large effect on the shape of the interface and the condensation rate across the interface [3,9].

Stagnant or moving water is surrounding the steam plume and hot water layer. As shown by Celata et al. [9], the water velocity directly effects the turbulence in the hot water layer and consequently the steam plume shape and the heat transfer coefficient. Steam condensing in water also generates a temperature distribution in water [17].

Dependent on the inflow conditions, the surrounding water can be a one or a two-phase water with uncondensed steam bubbles. Downstream of the condensation region a self-similar jet is developed in the water. Experimental observations have shown that the surrounding water is directly affected by the formation and collapse of the steam plume, resulting in pressure oscillations in water [2,5,12,14,16].

2.2. Regimes of DCC

The dynamic behaviour and the geometrical appearance of the steam plume is subdivided in three main regimes:

- Chugging regime.
- Jetting regime.
- Bubbling regime.

The chugging regime is characterised by a flat or curved shape of the steam plume located in the injector, and the

steam plume size is close to the injector's cross-sectional area. The chugging regime occurs at steam inflow rates up to 80 kg/(m^2 s), depending on the surrounding water temperature and steam injector diameter. The location of the steam plume in the injector may vary continuously moving from the outer edge of the injector into the injector and backwards. Chugging occurs because the steam inflow rate is smaller than the condensation rate which causes suction of surrounding water into the steam injector. If chugging occurs inside the injector in a pulsating manner, the condensation is called interfacial condensation oscillation. For this type of condensation the steam inflow rate is normally smaller than 5 kg/(m^2 s).

For steam inflow rates higher than about 100 kg/(m^2 s), steam forms a plume which holds approximately constant size and shape during the course of the experiment. This type of condensation is called jetting regime. Jetting consists of three main plume shapes which include: conical, ellipsoidal and divergent shape. For some inflow conditions close to the bubbling regime, the plume can also take a hemispherical shape. The length of the plume in the jetting regime can vary from 1 mm to more than 15 cm. If the condensation occurs in conical or ellipsoidal jetting regime, the plume will take a regular shape with a smooth surface. For water temperatures higher than 70–80 °C, the plume will take an irregular divergent shape. This regime is named divergent jetting. The length of a divergent plume is usually bigger than 2 cm.

For steam inflow rates between chugging and jetting, bubbling occurs. Here, injected steam generates a regular or an irregular bubble at the edge of the injector. The generated bubble grows and when a maximum size of the bubble is reached, the whole or a part of the bubble is detached from the injector. The remaining part of the original bubble starts to grow until a maximum bubble size is reached. In certain cases there is a collapse of the original bubble after detachment. Detached parts of the bubble are dragged away from the steam injector and continue to condense, generating a trace of smaller steam bubbles in the downstream flow.

3. Three-dimensional condensation regime diagram

Comparison of the two-dimensional regime maps shows that all maps hold similar features, however, steam and water conditions can vary significantly as well as the regime pattern. Distinct variations are seen when comparing the regime maps from different injector diameters. Fig. 2 provides a detailed plot of three regime maps obtained with different injector sizes. The figure clearly indicates a lack of proportionality and the regime map is not scalable from one injector size to another size if there is a substantial change in injector size. For example, while the regime map provides a distinct chugging regime with large injector diameters, chugging is marginal with a comparatively small injector diameter. This observation is very significant and implies that the regime map can not be normalised with respect to injector size; hence, a single two-dimensional regime map is unsuitable for a wide range of injector sizes. A further aspect of consideration is the injector shape. However, studies on the injector shape reported by [1,17] are inconclusive. Furthermore, the majority of studies on DCC are performed using a cylindrical shape injector.

For this reason a new three-dimensional condensation regime diagram is developed. The traditional dependencies of steam mass inflow rate (G_0) and water subcooling ($\Delta T = T_s - T_w$) are used. Based on the above analysis the injector diameter (D) is selected as a third dependency. Other definitions for the regime dependencies have been studied, but provided very poor correlation. The data for

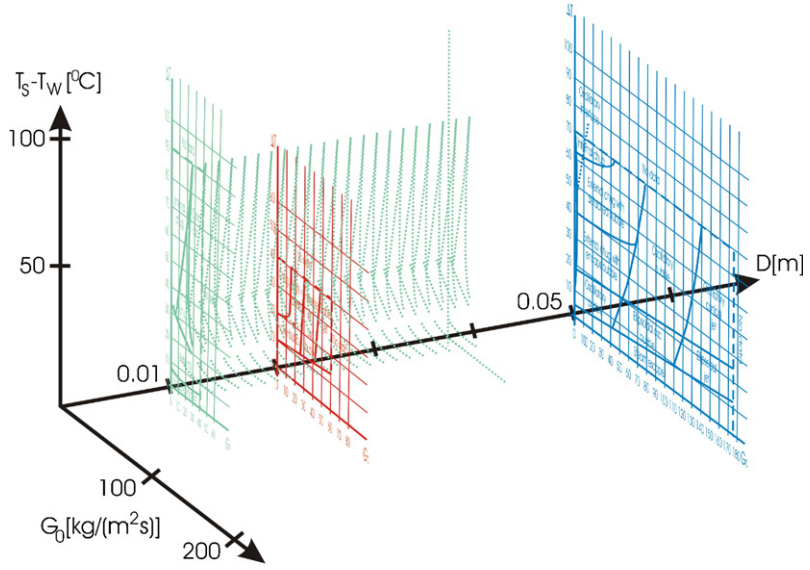

Fig. 2. A three-dimensional diagram of regime maps. Each colour presents a regime map from different researchers. In blue colour is a regime map from Chan and Lee [2], in red is a regime map proposed by Liang and Griffith [3] and in green colour regime map by Aya and Nariai [14].

the 3DCR diagram was obtained from a large number of independent studies published during the last three decades [1–4,6,7,10,12,14–16].

Fifteen different regimes were identified, all reported at slightly different flow conditions. For low temperature subcooling (ΔT approximately 10 °C or less) no condensation was detected. Under these conditions, the temperature difference between steam and surrounding water is too small for the steam to condense before it escapes from the water. At high steam inflow rates ($G_0 > 300$ kg/(m^2 s)) and small temperature differences ($\Delta T < 35$ °C) divergent jetting was reported. At similar steam inflow rates, but with medium to high water subcooling ($\Delta T > 35$ °C) ellipsoidal jetting was reported. Conical jetting was reported at medium steam inflow rates (120 kg/(m^2 s) $< G_0 <$ 300 kg/(m^2 s)) across a range of temperature differences. At small steam inflow rates (2 kg/(m^2 s) $< G_0 <$ 60 kg/(m^2 s)) and temperature differences above 20 °C a series of different chugging regimes were reported. These are internal chugging, small chugging, external chugging with detached bubbles and external chugging with encapsulating bubbles. They were reported at slightly different conditions. Furthermore, some researchers reported only some of the chugging regimes. At very small steam inflow rates ($G_0 < 2$ kg/(m^2 s)) interfacial condensation oscillation was reported. Various forms of bubbling regimes were reported for conditions between the chugging regime and the conical jetting regime (60 kg/(m^2 s) $< G_0 <$ 120 kg/(m^2 s)), and for conditions between the chugging regime and no condensation area (5 °C $< \Delta T <$ 20 °C at 1 kg/(m^2 s) $< G_0 <$ 60 kg/(m^2 s)). A range of different bubbling regimes were reported and included: oscillatory bubbling, ellipsoidal oscillatory bubbling, low frequency bubbling, high frequency bubbling, bubbling condensation oscillation and condensation oscillation.

For a clearer description of condensation the data was rationalised. All different chugging regimes were grouped together in one chugging regime and similarly also all bubbling regimes were grouped into one bubbling regime. The jetting regimes cover a large range of flow conditions and give important information about the steam plume shape; hence, the jetting regime was subdivided into three jetting regimes. Rationalisation of the regime data resulted in a total of seven different regimes. These include: no condensation area, interfacial condensation oscillation, chugging regime, bubbling regime, divergent jetting, ellipsoidal jetting and conical jetting.

The 3DCR diagram was created from three-dimensional surfaces representing the outer borders of the condensation regime. All surfaces were placed in a single diagram to form a new three-dimensional condensation regime diagram for DCC of steam injected into stagnant water. The 3DCR diagram is presented in Fig. 3. It presents areas of different regimes for different steam inflow rates in the range from 0 kg/(m^2 s) to 1500 kg/(m^2 s), for steam injector diameter sizes between 0.00135 m and 0.5 m and for a water subcooling ranging from 0 °C to 90 °C. For water subcooling between 90 and 100 °C data was not available. The diagram clearly shows areas of different jetting regimes: conical jetting, ellipsoidal jetting and divergent jetting. Jetting regimes cover most of the new 3DCR diagram and they appear at steam inflow rates around 200 kg/(m^2 s)

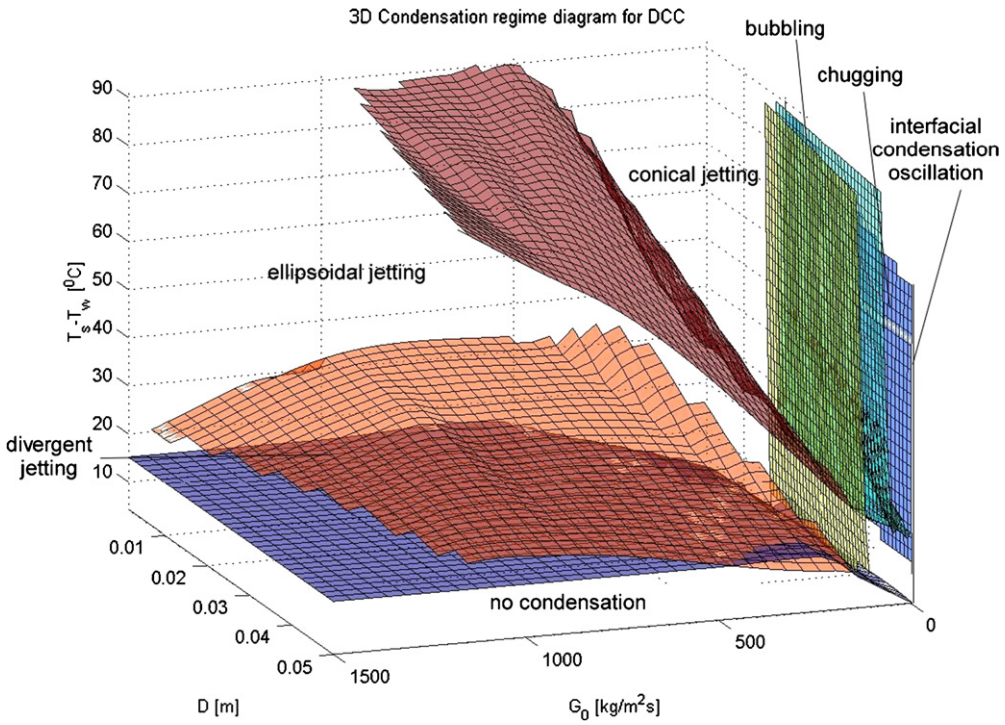

Fig. 3. New 3DCR diagram viewed from a side with large steam injector diameters.

and proceed to high steam inflow rates. In the jetting area it can be seen that the divergent jetting appears above the no condensation area and covers a section of the jetting area that ranges from approximately 10 °C to 25 °C water subcooling, depending on a steam injector diameter. Above the divergent jetting area, an ellipsoidal jetting area can be observed. It expands to high water subcooling at steam inflow rates higher than 1000 kg/(m^2 s). At lower steam inflow rates, this area is diagonally cut with an area of conical jetting, which occurs at a water subcooling around 25 °C at 200 kg/(m^2 s) and expands to 90 °C at 200 kg/(m^2 s). For steam inflow rates smaller than 200 kg/(m^2 s) bubbling, chugging and interfacial condensation oscillation occur (Fig. 4). For very small steam inflow rates up to 2 kg/(m^2 s) interfacial condensation oscillation is ranging from 15 °C to 60 °C water subcooling. The chugging regime starts when the water subcooling is 20 °C and extends to 90 °C and covers an area of the regime map up to a steam inflow rate of 50 kg/(m^2 s). With lower water subcooling a bubbling regime is observed. For steam inflow rates between 50 kg/(m^2 s) and 120 kg/(m^2 s) a bubbling regime is observed with water subcooling up to 90 °C

To ensure sufficient accuracy of the new 3DCR diagram, the diagram is constructed such that areas with insufficient data remain white.

3.1. Evaluation

The new 3DCR diagram was evaluated with data presented in Table 1. This data was not used during creation of the diagram. The results were added to the 3DCR diagram and compared with predictions for regimes from the diagram (Figs 5–7).

Table 1
Data used for validation of the new 3DCR diagram

Data from	$G_0\left[\frac{kg}{m^2 s}\right]$	D [m]	ΔT [°C]	Regime
Kim and Song [11]	337	0.00765	78	Conical jetting
Kim and Song [11]	468	0.00765	74	Ellipsoidal jetting
Experiments	1105	0.004	85	Ellipsoidal jetting
Youn et al. [5]	60 to 80	0.02	>30	Transition
Youn et al. [5]	<60	0.02	20	Bubbling

Fig. 5 shows two different sections of the new 3DCR diagram together with data for evaluation from Kim and Song [11]. The sections relate to steam inflow rates up to 800 kg/(m^2 s) and for a water subcooling temperature of 78 °C (Fig. 5a) and 74 °C (Fig. 5a). For these temperatures Kim and Song [11] reported two regimes, conical jetting and ellipsoidal jetting. Their data is added to the graph and presented in the form of stars. The figures show that both stars are predicted correctly by the 3DCR diagram. The graph in Fig. 6 shows a cross-section of the new 3DCR diagram for steam inflow rates up to 1200 kg/(m^2 s) and for a water subcooling temperature of 85 °C. An ellipsoidal jet observed during experiments is represented by a star that is predicted accurately by the 3DCR diagram. The graph suggests that with an extension of the conical–ellipsoidal jetting regimes boundary predicted by the 3DCR diagram to smaller injector sizes D, data will fall into the ellipsoidal jetting regime, which was also observed in the experiment. More data is needed for a solid proof, however this evaluation indicates, that the new

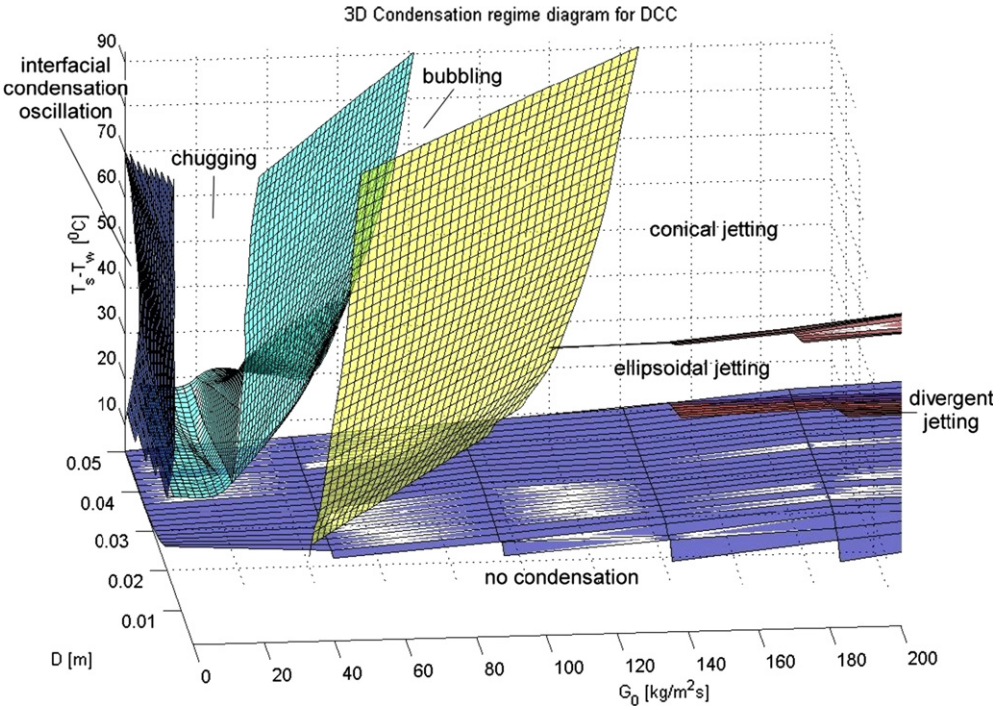

Fig. 4. Side view of a section of the new 3DCR diagram at low steam inflow rates. View from a side with small steam injector diameters.

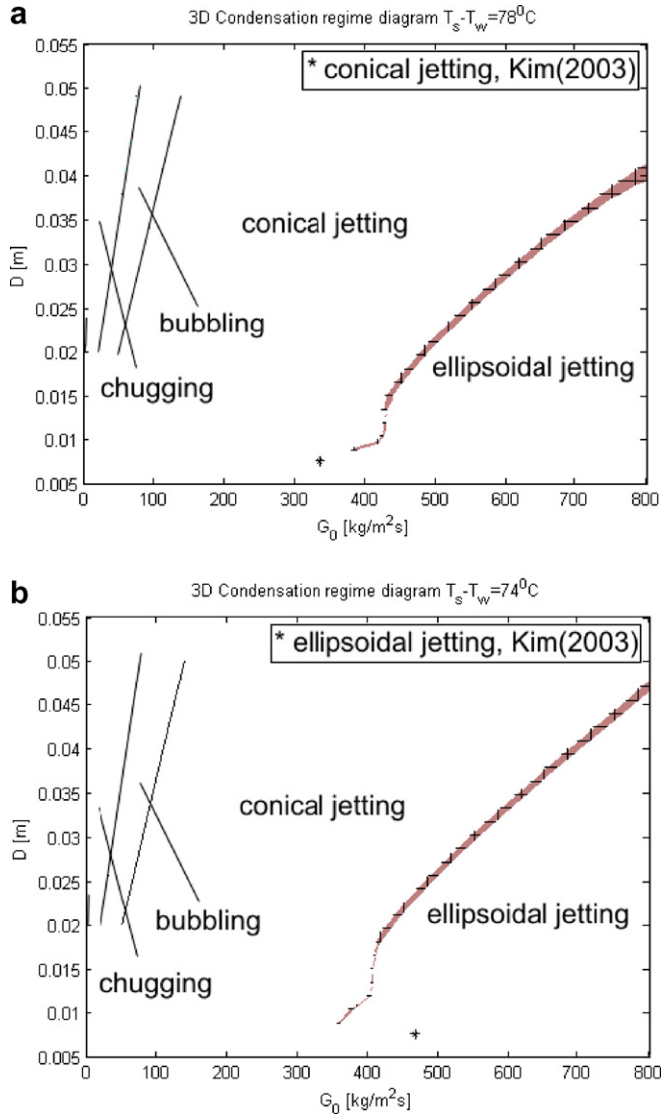

Fig. 5. Comparison between the new 3DCR diagram and data for validation from Kim and Song [11]. (a) Star relates to data for a conical jetting regime $G_0 = 337$ kg/(m^2 s), $D = 0.00765$ m, $\Delta T = 78$ °C. (b) Star relates to data for an ellipsoidal jetting regime $G_0 = 468$ kg/(m^2 s), $D = 0.00765$ m, $\Delta T = 74$ °C.

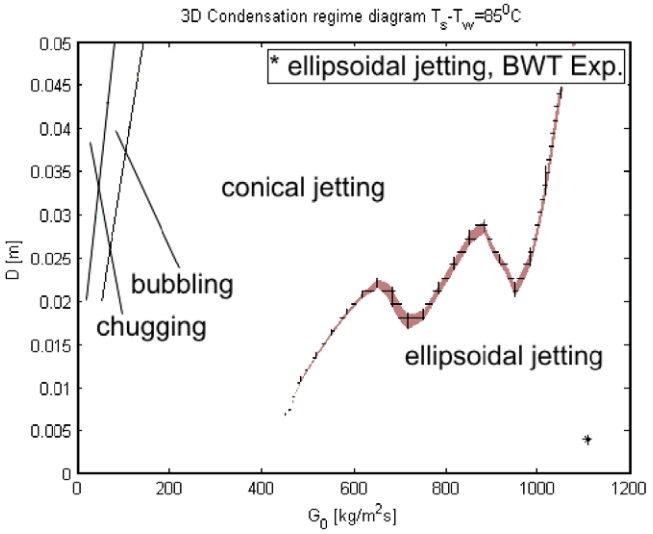

Fig. 6. Comparison between the new 3DCR diagram and data for validation obtained during the development of the BWT system. Star relates to data for an ellipsoidal jetting regime $G_0 = 1105$ kg/(m^2 s), $D = 0.004$ m, $\Delta T = 85$ °C.

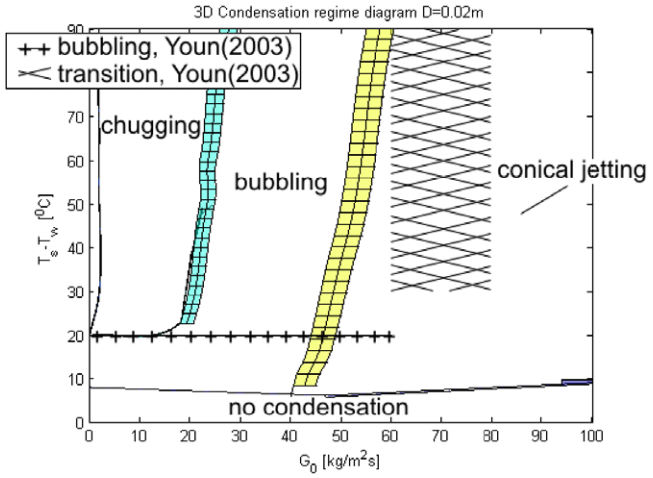

Fig. 7. Comparison between the new 3DCR diagram and data for validation from Youn et al. [5]. Line with crosses relates to data for a bubbling regime $G_0 > 60$ kg/(m^2 s), $D = 0.02$ m, $\Delta T = 20$ °C. Shaded area relates to data for transition $G_0 \in (60, 80)$ kg/(m^2 s), $D = 0.02$ m, $\Delta T > 30$ °C.

3DCR diagram is likely to be valid for steam inflow rates in the jetting regime and it can also be extended into a 'white' area of settings.

More data is required for evaluation of the diagram at small steam inflow rates. For this reason, data from Youn et al. [5] was used. During Youn's experiments small steam inflow rates were used, and the regimes were detected by measurement of the pressure pulses in the water flow. For identification of the various regimes they used information from literature. Youn et al. reported two different transitions between regimes (Table 1). Fig. 7 shows a section of the new 3DCR diagram for steam inflow rates up to 100 kg/(m^2 s) and steam injector diameter of 0.02 m compared with data from Youn et al. [5]. The data from Youn et al. does not entirely correspond with data from the 3DCR diagram and the prediction of transition from bubbling to jetting regime is under-predicted by the diagram by approximately 15% as compared to data from Youn et al. [5]. Further data for bubbling regime show agreement, however, Youn et al. reported the bubbling regime to extend to slightly higher steam flow rates as compared to 3DCR diagram at reported flow conditions. Nevertheless, the results from the 3DCR diagram are in general agreement.

More experimental data is required to evaluate the new 3DCR diagram in the chugging and bubbling regimes. Furthermore, more experiments should be performed to show the relation between pressure pulses and condensation regimes.

4. DCC into a water flow

In addition to flow conditions and injector size, condensation of steam is affected by the movement of the water. In the 3DCR diagram, presented in chapter 3 the water was assumed stagnant, however, if a water flow is applied there is a constant supply of fresh cold water. Therefore, the regime diagram may well predict different if a water flow is applied. It is expected that a separate three-dimensional condensation regime diagram is required for condensation of steam in a water flow.

The experiments performed in connection with this study were aimed to investigate the steam behaviour in a water flow. As part of the experiment steam was injected in the centre of a water flow with a centerline velocity of 1.9 m/s and a water subcooling of 85 °C. The steam inflow rate was less then 5% of the water flow in the pipe to ensure blockage effects were negligible. Observations showed three different regimes of condensation. For a steam inflow rate of 424.4 kg/(m^2 s) and an injector with 5 mm diameter, a hemispherical steam plume occurred at the exit of the injector (Fig. 8a). With an injection of 663.1 kg/(m^2 s) of steam through an injector with 4 mm diameter the steam plume became conically shaped (Fig. 8b). For steam injectors smaller then 2 mm and a steam inflow rate of 2652.6 kg/(m^2 s) ellipsoidal jetting was seen (Fig. 8c). Corresponding diagrams of the plume are added to photographs in Fig. 8.

The observations from these experiments were compared with the predictions from the 3DCR diagram. Fig. 9 shows a cross-section of the new 3DCR diagram with a water subcooling of 85 °C. The regime names are added to the graph and black markers representing the experimental observations are added. The circular marker presents the data from a 5 mm injector. The marker is located in the vicinity of the transition from conical to ellipsoidal jetting. However, the experiments in a water flow suggested a hemispherical steam plume (Fig. 8a). Such steam plume is expected to occur in the transition region between bubbling and conical jetting. The square shaped marker presents data from a 4 mm injector. The marker is located in the first part of the ellipsoidal jetting regime. However, the experiments provided a conical jet

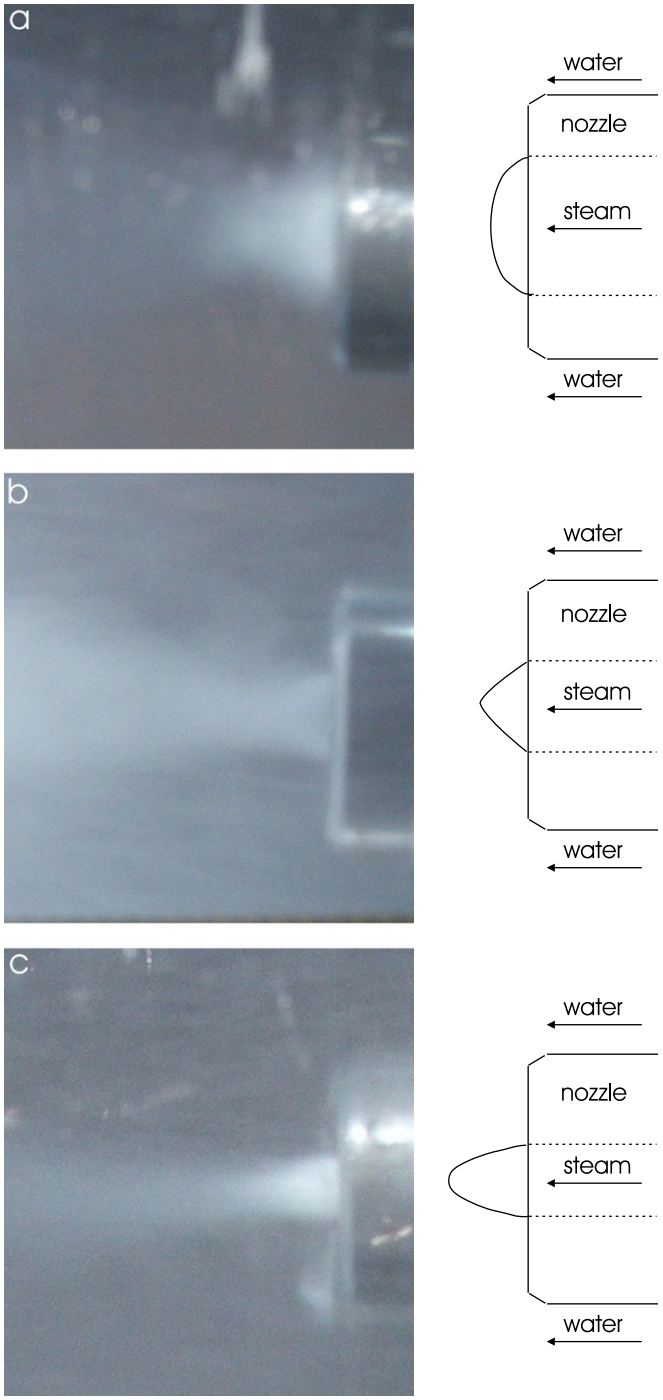

Fig. 8. Steam plume injected into a water flow with velocity 1.9 m/s and water subcooling 85 °C. (a) Hemispherical plume, $D = 5$ mm, $G_0 = 424.4$ kg/(m^2 s), (b) conical plume, $D = 4$ mm, $G_0 = 663.1$ kg/(m^2 s), (c) ellipsoidal plume, $D = 2$ mm, $G_0 = 2652.6$ kg/(m^2 s).

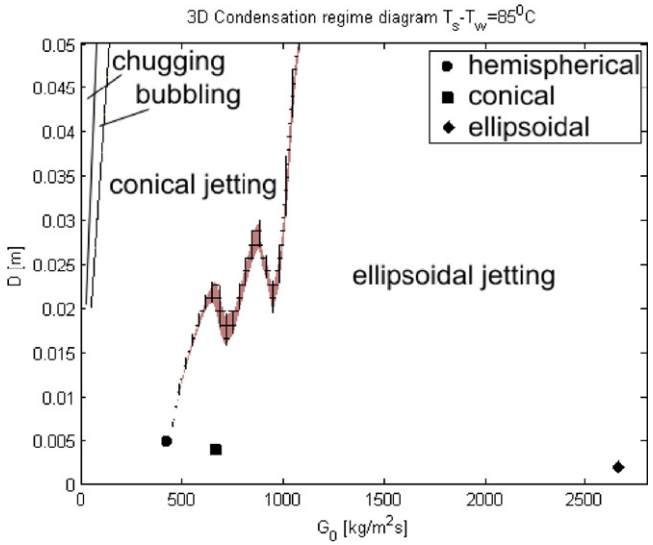

Fig. 9. 3DCR diagram for DCC of steam into a stagnant water at $T_s - T_w = 85$ °C with added data for DCC into a water flow, obtained during experiments.

(Fig. 8b). The final diamond shaped marker presents the data from a 2 mm injector. The marker is located in the ellipsoidal jetting regime, and an ellipsoidal jet was also found in the experiments (Fig. 8c).

It is concluded that a new 3DCR diagram for DCC of steam in a water flow holds similar features to the proposed 3DCR diagram for stagnant water. However, it is expected that the location of the various regimes in the diagram differs. More experiments at different flow conditions should be performed to make some conclusive comments.

5. Conclusions

In the paper a new three-dimensional condensation regime diagram for DCC of steam injected into a stagnant water was presented. The 3DCR diagram can predict the DCC regimes across a wide range of flow conditions and injector sizes. This is an advantage from the two-dimensional regime maps found in literature. The two-dimensional regime maps are able to predict the regimes for one injector size only. The new 3DCR diagram was created from experimental data found in literature. The experimental data was independent and published over a period of more then three decades. The author is not aware of any further work published on this subject that could enhance the diagram.

The 3DCR diagram was evaluated with data not used for creation of the diagram. The evaluation showed that the 3DCR diagram is accurately predicting the various jetting regimes. Furthermore the transition regions between the various regimes can be extended if more experimental data can be provided. More experimental data is needed for firm evaluation of the diagram, especially in the chugging and bubbling regimes. If more data is available this may result in minor modifications to the 3DCR diagram, however, the general structure of the diagram is well established as general trends are predicted accurately.

More experimental data is required to construct a three-dimensional condensation regime diagram for steam injected into a water flow.

Acknowledgements

The photographs presented are from experiments performed at Metafil AS, Norway and Det Norske Veritas, Norway. Authors thankfully acknowledge permission to use their experimental material.

References

[1] P.J. Kerney, G. M Faeth, D.R. Olson, Penetration characteristics of a submerged steam jet, AIChE J. 18 (3) (1972) 548–553.
[2] C.K. Chan, C.K.B. Lee, A regime map for direct contact condensation, Int. J. Multiphase Flow 8 (1) (1982) 11–20.
[3] K.S. Liang, P. Griffith, Experimental and analytical study of direct contact condensation of steam in water, Nucl. Eng. Des. 147 (1994) 425–435.
[4] Y.S. Kim, J.W. Park, Determination of the steam–water direct contact condensation heat transfer coefficient using interfacial transport models, Proc. Am. Nucl. Soc. – Therm. Hydraulics Div. 10 (1997) 110–117.
[5] D.H. Youn, K.B. Ko, Y.Y. Lee, M.H. Kim, Y.Y. Bae, J.K. Park, The direct contact condensation of steam in a pool at low mass flux, J. Nucl. Sci. Technol. 40 (10) (2003) 881–885.
[6] Y.S. Kim, J.W. Park, C.H. Song, Investigation of the steam–water direct contact condensation heat transfer coefficient using interfacial transport models, Int. Commun. Heat Mass Transfer 31 (3) (2004) 397–408.
[7] H.Y. Kim, Y.Y. Bae, C.H. Song, J.K. Park, S.M. Choi, Experimental study on stable steam condensation in quenching tank, Int. J. Energy Res. 25 (2001) 239–252.
[8] L.D. Chen, G.M. Faeth, Condensation of submerged vapor jets in subcooled liquids, Trans. ASME, J. Heat Transfer 104 (1982) 774–780.
[9] G.P. Celata, M. Cumo, G.E. Farello, G. Focardi, Direct contact condensation of steam on slowly moving water, Nucl. Eng. Des. 96 (1986) 21–31.
[10] M.H. Chun, Y.S. Kim, J.W. Park, An investigation of direct condensation of steam jet in subcooled water, Int. Commun. Heat Mass Transfer 23 (7) (1996) 947–958.
[11] Y.S. Kim, C.H. Song, Overall review of steam jet condensation in a next generation reactor water pool, in: Proceedings of IMECB'03, ASME, 2003, pp. 1–10.
[12] J.A. Block, Condensation-driven fluid motions, Int. J. Multiphase Flow 6 (1980) 113–129.
[13] A. Petrovic, Analytical study of flow regimes for direct contact condensation based on parametrical investigation, J. Pressure Vessel Technol. 127 (1) (2005) 20–25.
[14] I. Aya, H. Nariai, Boundaries between regimes of pressure oscillation induced by steam condensation in pressure suppression containment, Nucl. Eng. Des. 99 (1987) 31–40.
[15] I. Aya, H. Nariai, Evaluation of heat-transfer coefficient at direct-contact condensation of cold water and steam, Nucl. Eng. Des. 131 (1991) 17–24.
[16] M.E. Simpson, C.K. Chan, Hydrodynamics of a subsonic vapor jet in subcooled liquid, J. Heat Transfer 104 (1982) 271–278.
[17] R.J.E. van Wissen, K.R.A.M. Schreel, C.W.M. van der Geld, J. Wieringa, Turbulence production by a steam-driven jet in a water vessel, Int. J. Heat Fluid Flow 25 (2004) 173–179.